2006

Model for the steady-state growth of porous anodic alumina films

Jerrod E. Houser
Iowa State University

Kurt R. Hebert
Iowa State University, krhebert@iastate.edu

Model for the steady-state growth of porous anodic alumina films

Abstract
Simulations were developed for the distributions of electrical potential and incorporated anions in porous anodic alumina (PAA) films during steady-state growth. Predictions of a model for the potential distribution based on Laplace's equation were compared to those of the current continuity equation in conjunction with high-field conduction. It was found that Laplace's equation, which has been used previously in PAA models, resulted in strong violations of charge conservation, when the current density was evaluated using the high field conduction equation. Interface motion predicted by the current continuity equation was nearly uniform except near convex ridges on the metal-film interface. This model was extended to predict the distribution of anions in the film, since incorporated anions may provide suppression of conduction near the ridge. The spatial distribution of acid anions predicted by the model agreed with experimental observations.

Keywords
acid anions, charge conservation, current continuity, high-field conduction, interface motion, Laplace's equations, metal film interfaces, porous anodic alumina (PAA) films

Disciplines
Biochemical and Biomolecular Engineering | Biological Engineering

Comments
The archival version of this work was published in J. E. Houser and K. R. Hebert, "Model for the Steady-State Growth of Porous Anodic Alumina Films", *ECS Trans.,* **3**, (31) 375-385 (2007). doi: 10.1149/1.2789243

ECS Transactions, 3 (31) 375-385 (2007)
10.1149/1.2789243, copyright The Electrochemical Society

Model for the Steady-State Growth of Porous Anodic Alumina Films

Jerrod E. Houser and Kurt. R. Hebert

Department of Chemical & Biological Engineering, Iowa State University, Ames, Iowa 50011

Simulations were developed for the distributions of electrical potential and incorporated anions in porous anodic alumina (PAA) films during steady-state growth. Predictions of a model for the potential distribution based on Laplace's equation were compared to those of the current continuity equation in conjunction with high-field conduction. It was found that Laplace's equation, which has been used previously in PAA models, resulted in strong violations of charge conservation, when the current density was evaluated using the high field conduction equation. Interface motion predicted by the current continuity equation was nearly uniform except near convex ridges on the metal-film interface. This model was extended to predict the distribution of anions in the film, since incorporated anions may provide suppression of conduction near the ridge. The spatial distribution of acid anions predicted by the model agreed with experimental observations.

Introduction

Porous anodic alumina (PAA) films are formed by anodic polarization of aluminum in baths of, for example, sulfuric, oxalic or phosphoric acid (1-3). The morphology of PAA consists of evenly spaced and mutually parallel pores, oriented perpendicular to the metal/film interface. Viewed from the top, the pores form a hexagonal array. The interpore distance ranges from 10 to 500 nm, and along with the pore diameter may be controlled by the film formation voltage and the acid type.

There is yet no generally accepted quantitative mechanism for porous film formation. Qualitative explanations for PAA growth have been advanced based on concepts such as electric field and temperature-enhanced dissolution of the oxide at the pore bottom, and nonuniform mechanical stress along the metal/film interface (4-6). Models for porous alumina have been developed based on descriptions of ion transport and interfacial reactions, and on the coupling of interfacial reactions and transport with elastic stress and surface energy (7-9). These models were based on the potential distribution in the film, which was determined by Laplace's equation following the assumption of zero space charge in the film. However, it is not clear that Laplace's equation offers a valid description of the potential distribution. An alternative approach is to apply the current continuity, or charge balance differential equation, coupled with the high-field conduction law normally obeyed by anodic films. A one-dimensional model of this type was found to yield reasonable current-potential relations for anodizing (10).

Here we compare models for the potential distribution in porous anodic alumina during steady-state film growth. Potential distributions were predicted based on either Laplace's equation (based on the assumption of no space charge) or the current continuity

equation coupled with high field conduction. The potential distributions were used to calculate the local rates of motion of the metal-film and film-solution interfaces. These predictions were evaluated with respect to the requirement of uniform interface motion (i. e., time-invariant interface profiles) during steady-state film growth. More details of the modeling approach can be found in Ref. 11.

Model

Potential Distribution

As mentioned above, two cases were investigated with the model. The first model assumes that the potential distribution is determined by the current continuity equation, $\nabla \bullet \mathbf{i} = 0$. At the high electric fields approaching 1 V/nm in the oxide, the ionic conduction current density fluxes follow the high-field conduction law, in which the current increases exponentially with electric field. The resulting current continuity equation is

$$\nabla \bullet \left(\frac{\sinh\left(B|\nabla\phi|\right)}{|\nabla\phi|} \nabla\phi \right) = 0 \qquad [1]$$

The second model assumes that the potential distribution is governed by electrostatics, and that there is zero space charge in the oxide. In this case, the potential distribution obeys Laplace's equation,

$$\nabla^2 \phi = 0 \qquad [2]$$

Eqs. 1 and 2 become equivalent only for a planar one-dimensional film geometry (when either equation yields a uniform field), or for multidimensional geometries when the field is small (since Eq. 1 reduces to Laplace's equation). Since the application to porous anodic films falls well outside these restrictions, the potential fields predicted by the two equations are significantly different. Eq. 2 has been used in previous models of PAA films (7-9).

The simulation domain was the oxide surrounding a single pore in the film. In highly-ordered PAA films, the pores are parallel, circular in cross-section, and arranged in a two-dimensional hexagonal lattice. We approximated the hexagonal unit cell as a circle. Cross-sectional electron micrographs indicate that the metal-film interface at the pore bottom forms an approximately spherical contour (3, 4). However, close examination reveals that the film-solution interface is more accurately depicted by an elliptic surface, with a minimum film thickness along the pore axis. Fig. 1 shows model pore geometries, showing spherical (solid line) and elliptic (dashed line) film-solution interface contours, both of which were considered in calculations.

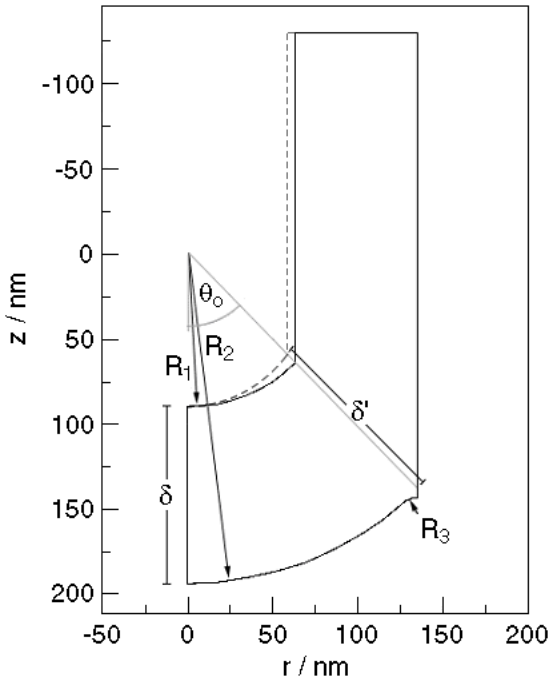

Figure 1. Outline of the model domain, representing a cross-section of the porous oxide formed in 0.4 M phosphoric acid at 25 °C. See text for descriptions of symbols. Dashed line indicates elliptic film solution interface profile, for δ'/δ larger than 1.

In Fig. 1, R_1 and R_2 are the radii of concentric spheres at the film-solution and metal-film interfaces, respectively. The other geometric parameters are θ_o, the angle from the pore axis to the ridge-top; R_3, the radius of curvature of the metal/film ridge-top; δ, the oxide thickness along the pore axis; and δ', the oxide thickness along the direction $\theta = \theta_o$. The ratio δ'/δ was 1.0 for the spherical film-solution interface, but ranged from 1.0 to 1.05 when elliptic interfaces were considered. This range was suggested by TEM cross section images of anodic films (3). Since the oxide is rotationally symmetric about the pore axis, the model domain included only half of the cross-section, as shown in Fig. 2. The calculations used a cylindrical coordinate system centered on the pore axis.

The boundary conditions were the same whether Eq. 1 or 2 was used to simulate the potential field in the film. The potential drop in the pore solution was neglected, so that the potential at the oxide-solution interface was set to the reference value of zero. The potential at the metal-film interface along the bottom of the domain was then V, the applied anodizing voltage. Because of symmetry, zero flux boundary conditions were applied at the left and right vertical edges of the domain.

During steady-state growth of porous alumina films, both interfaces of the film at the pore bottom maintain the same profile. Equations for the evolution of interface profiles were developed to test whether the model was consistent with this time-invariance. The velocity of the film/solution interface is determined by a balance on oxygen ions across the interface, which accounts for deposition of oxygen ions from solution and removal of these ions by migration into the film.

$$v_{n,fs} = (t_O - \varepsilon)\frac{i_{n,fs}}{6FC_{ox}} \qquad [3]$$

where C_{ox} is the molar concentration of the oxide, $i_{n,fs}$ is the component of the conduction current density normal to the interface, t_O is the transport number for the oxygen species in the oxide, and ε is the current efficiency for oxide formation at the interface. The normal velocity at the metal-film interface is also based on an oxygen balance, which in this case includes only the arrival of O^{-2} ions by migration across the film,

$$v_{n,mf} = t_O \frac{i_{n,mf}}{6FC_{ox}} \qquad [4]$$

The time derivatives of each interface profile, $z_{fs}(r,t)$ *and* $z_{mf}(r,t)$, are related to the respective normal velocities by

$$\frac{\partial z}{\partial t} = v_n \left[1 + \left(\frac{\partial z}{\partial r} \right)^2 \right]^{1/2} \qquad [5]$$

In calculations of $\partial z_{fs} / \partial t$, the current efficiency ε was approximated as a constant, independent of position.

Incorporation of Acid Anions

As the results in the next section will show, ionic conduction alone in a pure oxide is unable to predict a time-invariant interface evolution profile for an experimentally observed steady-state geometry. The acid used during anodizing, along with the voltage, determines the geometric parameters of PAA (6, 12). The incorporation of acid anions into the films has been extensively documented (13-15). Since these considerations suggest that incorporated anions likely play a key role in the growth mechanism, an extended model was developed including the species continuity equation for the acid anion. Unlike the models in the previous section, the extended model incorporated the constraint that the metal-film interface velocity was uniform. The potential distribution at the metal film interface was predicted, and compared to the known constant potential. The reference frame in the extended model was not stationary, but instead moved with the uniform interface velocity.

The anion flux included contributions from both diffusion and ionic migration,

$$\mathbf{J_A} = -D_A \nabla C_A + C_A (\alpha \mathbf{v}_m + \mathbf{v}) \qquad [6]$$

In the convective term, $\mathbf{v}_m$ is the oxygen migration velocity according to the high field conduction law, α is the ratio of the acid anion transport number to that of oxygen, and hence $\alpha \mathbf{v}_m$ is the anion migration velocity. $\mathbf{v}$ is a pseudo-convective velocity, equal and opposite to the uniform interfacial velocity in the laboratory frame. The potential significance of diffusive transport during anodizing was demonstrated by Pringle, in studies of tantalum oxide films using noble metal atom and ^{18}O tracers (16,17). While Pringle's results showed that diffusion is current-driven, Eq. 6 models diffusion as if it were thermally activated. Recently, significant broadening of the depth profiles of incorporated phosphate, oxalate and sulfate ions in anodic alumina films has been

detected, as would result from a diffusive contribution to transport (18-20). These are the same anions most frequently used in acid anodizing baths. Application of continuity yielded a differential equation to be solved along with the current continuity equation (Eq. 1),

$$\nabla \bullet \mathbf{J}_A = 0 \qquad [7]$$

At the film solution interface, a continuity boundary condition for $\mathbf{J}_A$ was used, based on an anion incorporation rate proportional to the local current density. Zero flux conditions were applied normal to the vertical boundaries in Fig. 1, as well as at the metal film interface. As mentioned above, the boundary condition for the potential at the metal film interface was zero migration velocity normal to the interface. This constraint is equivalent to requiring time-invariance of the metal film interface profile, since v_n in Eq. 5 is zero.

Results and Discussion

The Potential Distribution and its Implications

All model equations were solved numerically with the finite element method, making use of the software application FEMLAB (24). Potential distributions calculated from Eqs. 1 and 2 alone are presented in Fig. 2. Compared to the uniform behavior of the current continuity case (right), the Laplace's equation case (left) reveals significant degrees of compaction of the isopotential lines along the film/solution interface at the pore bottom as well as near the ridge-top of the metal/film interface. In both regions the field strength was a factor of 4 larger than near the metal along the pore axis. The corresponding enhancement of current density, according to the high-field conduction equation, is 7 orders of magnitude. This nonuniformity is clearly incompatible with the requirement of uniform interface motion along the metal/film interface. Also, the combination of Laplace's equation and high field conduction results in a dramatic violation of current continuity. Thus, the requirement of zero space charge enforced by Laplace's equation is incompatible with the high field conduction law, typically exhibited in anodic films.

Unlike the predictions of Laplace's equation, the potential distribution from the current continuity equation is uniform over much of the scalloped region. Within this region, the field differs by only 10 % between the metal-film and film-solution interfaces. In view of the high sensitivity of the current density to electric field, only this small variation is needed to maintain the same net current at each interface. As in the Laplace's equation model, the field near the metal/film interface is locally increased on the ridge, but the degree of this enhancement is only 5%, much less than the relative increase from Laplace's equation. The relatively smaller effect of the ridge curvature is due to the high sensitivity of current density to electric field. The extension of current paths emanating from the metal-film interface into the pore wall region is therefore confined to the region close to the ridge, where the field enhancement is localized.

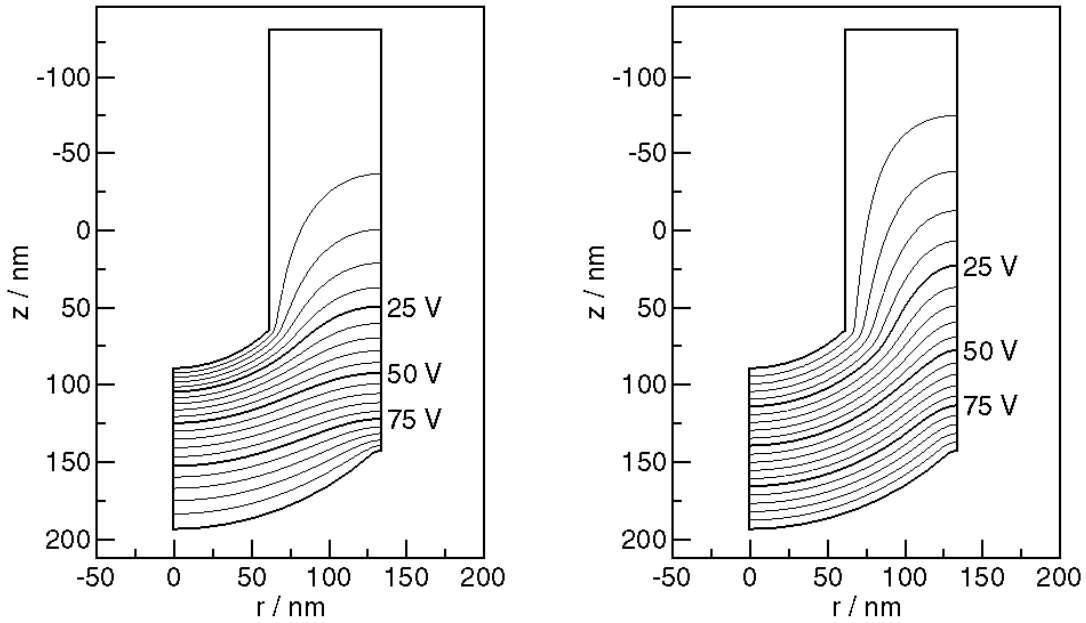

Figure 2. Contour plots of the potential distributions based on Laplace's equation (left) and current continuity equation (right). The film/solution and metal/film interfaces are at 0 and 100 V, respectively.

The current continuity equation requires that space charge be present in the oxide, as the potential does not satisfy Laplace's equation. Since the electric field near the pore axis is nearly constant and oriented along the axis, the space charge in this region can readily be estimated using Poisson's equation. The result is

$$\rho_e \cong -\frac{2K\varepsilon_o|\mathbf{E}|}{R} \qquad [19]$$

where R is the distance from the origin defined in Fig. 1 to a point in the film, K is the dielectric constant, and ε_o is the permittivity of free space. Using K = 10, $|\mathbf{E}|$ = 1 V/nm, and R = 150 nm, ρ_e is found to be equivalent to approximately 0.007 % of the charge density due to O^{-2} ions. This small amount of charge may be accommodated by non-stoichiometry, especially since Al surface oxides in aqueous solutions contain appreciable quantities of hydrogen, at least some of which is in the form of mobile protons (21, 22). Thus, mechanisms are likely available to adjust the space charge, in order to maintain the electric field distribution dictated by current continuity.

Fig. 3 shows the time derivatives of the metal-film interface profiles resulting from current continuity, with different values of the parameter δ'/δ describing the deviation of the film/solution interface from the spherical shape. Nearly uniform interface motion up to θ ~ 0.6 radian is obtained for δ'/δ = 1.023, a value within the range suggested by TEM cross sectional images of PAA films. This result strongly suggests that the elliptic shape of the film-solution interface is important for controlling the uniformity of the interface speed in the scalloped region. However, even at the optimum δ'/δ, the interface speed is locally high on the ridge, where the maximum value is about twice that on the scallop. Hence, fine adjustment of the interface geometry cannot resolve the local high interface

speed on the ridge itself, where the oxidation current density is intrinsically enhanced by the convex curvature.

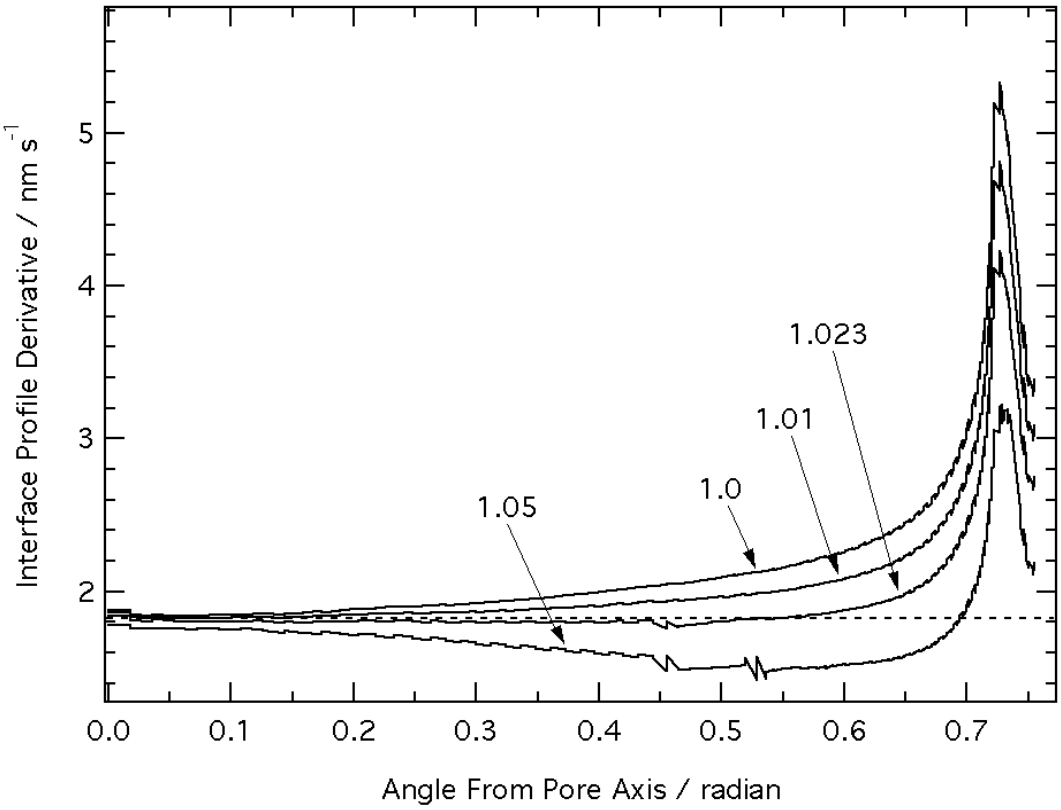

Figure 3. Time derivative of interface height profiles for various values of δ'/δ predicted by the current continuity equation. Field coefficient, *B*, set to 1.21×10^{-6} cm/V, an average of experimentally-obtained values; i_{ao} and ε were fit to 8.85×10^{-8} A/cm^2 and 0.46, respectively (11).

The transport processes and interfacial reactions contributing to PAA formation are illustrated in Fig. 4, which depicts the migration velocity vectors of Al^{+3} and O^{-2} ions, relative to a uniform reference velocity. The reference velocity was -**v**, where **v** is the local metal-film interface velocity at the pore axis. The figure shows that Al^{+3} ions formed at the metal-film interface directly under the pore migrate to the film-solution interface and are dissolved there, while those which form beneath the pore wall are incorporated into the accumulating oxide in the wall. As the O^{-2} ions formed at the film-solution interface migrate toward the metal interface, the downward component of the migration velocity diminishes due to spreading of the current vectors in the spherical-shaped film. Simultaneously, these ions move to the right with the horizontal component of the migration velocity. Eventually, the upward pseudo-convective velocity exceeds the downward component of migration, causing the O^{-2} ions to reverse direction and enter the pore wall region. Unlike models based on field-assisted dissolution, the present model based on migration accounts for both recession of the film-solution interface at the pore bottom, and also accumulation of oxide in the pore walls.

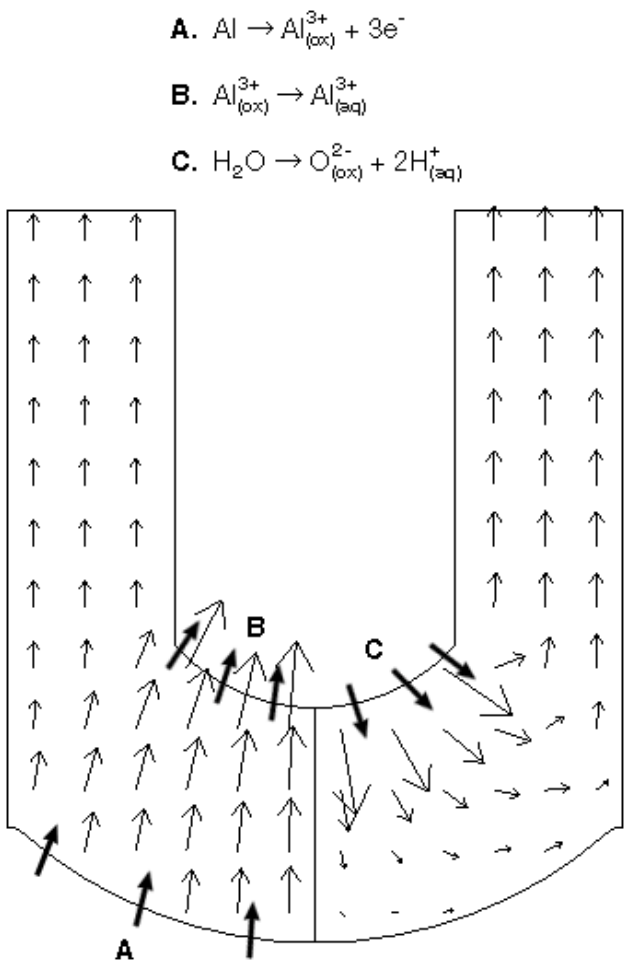

Figure 4. Ion migration velocities in the oxide film, predicted by the current continuity equation with $\delta'/\delta = 1.023$. Left side shows migration velocity vectors of Al^{+3} ions and right side those of O^{-2} ions. Interfacial reactions are labeled and indicated by bold arrows.

Acid Anion Distribution

Since the current continuity equation by itself does not predict a spatially uniform rate of interface motion, additional elements in the model are needed to completely justify the time-invariance of the film geometry. In particular, there should be an "inhibition" mechanism which preferentially reduces the local conduction current density near the ridge. Aside from anodizing voltage, the geometry of PAA films is strongly influenced by the nature of the anodizing acid (6, 12). Significant concentrations of the acid anion are incorporated into the outer portion of the barrier oxide at the pore base (13-15). The present preliminary communication does not propose a mechanism by which anions might inhibit conduction locally near the ridge. Instead, we present predicted anion concentration distributions, in order to demonstrate that they are reasonable with respect to experimental findings.

An example of the simulated distribution of acid anions is shown in Fig. 5. The geometry of the simulated PAA film accurately depicts that revealed by the TEM cross-sectional image in Fig. 27 (a) of Ref. 3. The dimensionless electric field and anion migration factor α used in the simulation are representative of experimental values (10,

18). The distribution exhibits the duplex structure observed experimentally, with a relative sharp transition between anion-containing and anion-free layers (23). The anions follow similar paths as oxygen ion trajectories in Fig. 4, except that the anions do not penetrate to the metal-film interface, owing their slow migration velocity relative to oxygen. The spreading of the acid anions in the upper part of the pore wall is due to the model's approximation of current-driven diffusion by thermally-activated diffusion. This approximation results in continued diffusion in the pore wall, despite the very small current density in this region. A more rigorous treatment of diffusion would result in preservation of the sharp duplex transition in the pore wall region. Nonetheless, the anion distribution closely reflects that suggested by TEM cross-section images (23).

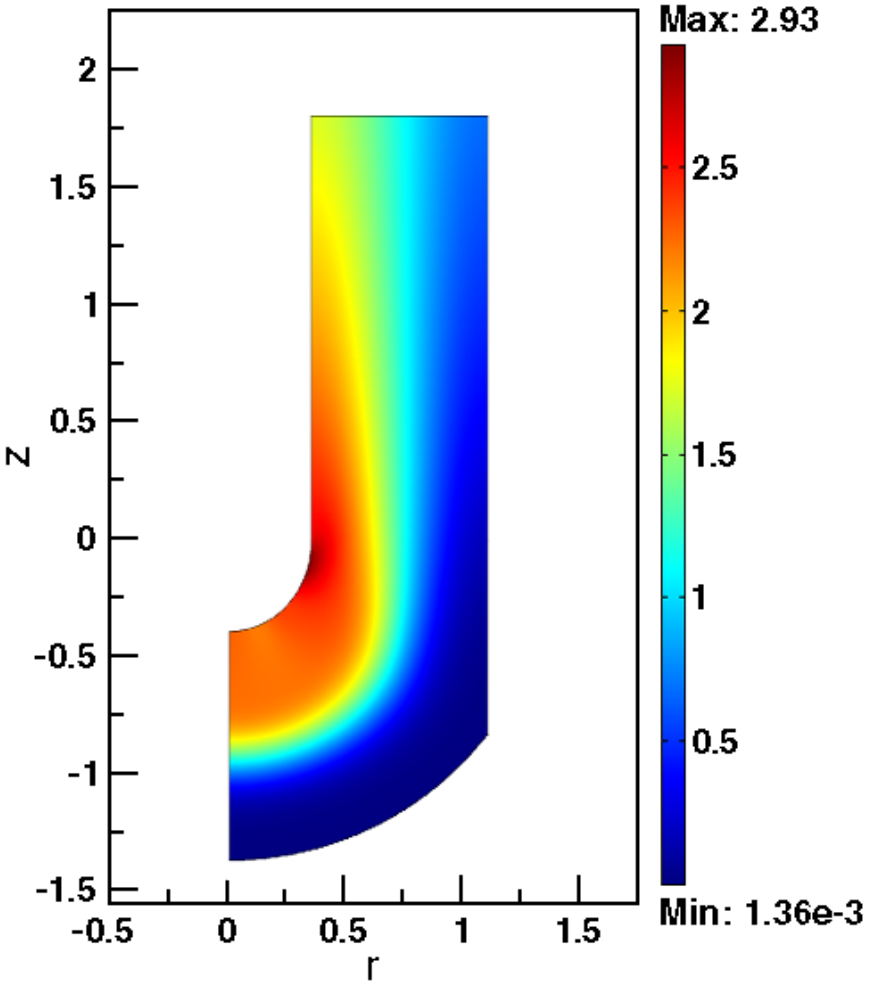

Figure 5. Distribution of dimensionless anion concentration in PAA film. z and r are normalized with respect to the barrier layer thickness δ. Geometric parameters are $R_2/R_1 = 3.55$, $\theta_o = 52.8^o$, $\delta'/\delta = 1.027$ (see Fig. 1 for definitions). Other parameters are $\alpha = 0.5$, $v\delta/D_A = 40$, $B|\nabla\phi| = 9.17$ at the metal/film interface along the pore axis.

By requirement of the boundary condition, the simulation has a time-invariant interface evolution profile. Fig. 6 shows the dimensionless potential profile along the metal/film interface that is required to meet this condition. The interface potential decreases by approximately 10 % near the ridge, owing to the enhancement of conduction by the local curvature. Of course, this variable potential differs from the uniform

potential which actually exists at the metal-film interface. One possible source of a potential drop near the ridge might be an interfacial space charge layer, at either the metal-film or film-solution interface. Previously, space charge layers associated with incorporated anions have been proposed to play an important role in the mechanism of PAA growth (14). At the film-solution interface, positive space charge would be created when the relatively large oxyanions absorb into multiple oxygen ion sites in the film.

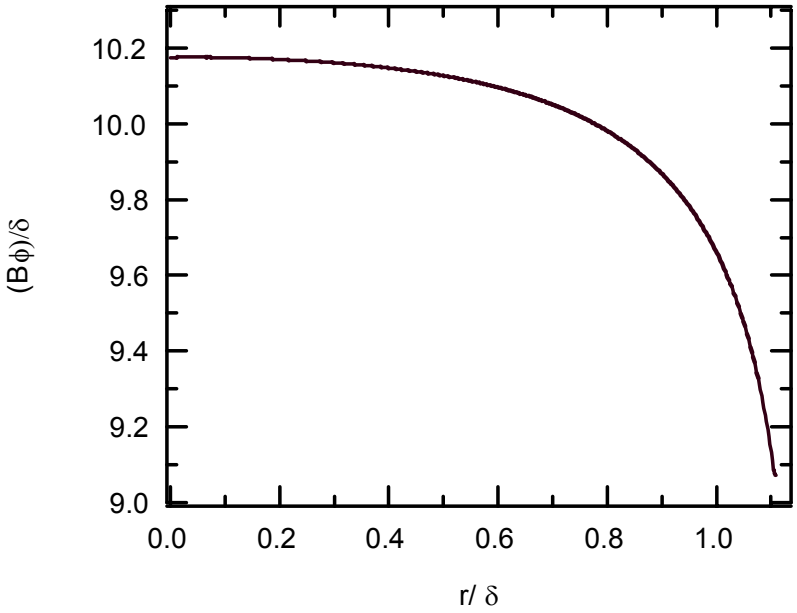

Figure 5. Distribution of dimensionless potential along the metal-oxide interface for the simulation shown in Fig. 4. See Fig. 1 for definitions of symbols.

Conclusions

A numerical simulation was developed for the electrical potential distribution in PAA films during steady-state growth, in order to help identify the physical and chemical processes responsible for the unique, highly ordered film morphology. Two approximate models of the potential were considered, one according to the assumption of no space charge in the film (Laplace's equation), and the other based on the current continuity equation coupled with high-field conduction. The predicted electric field in the film was then used to calculate the velocities of the metal-film and film-solution interfaces. The models were evaluated with respect to the requirement that the oxide geometry is time-invariant, and hence the interface motion should be uniform. Previous PAA models obtained the potential distribution from Laplace's equation.

Interfacial current densities calculated from the results of the Laplace's equation using the high-field conduction law exhibited non-physical behavior, including interface velocities varying by several orders of magnitude along the metal-film interface, as well as strong violations of charge conservation. On the other hand the current continuity equation produced uniform metal-film interface motion in the scalloped region, while the interface speed was enhanced by a factor of two near the ridge. The space charge density required to satisfy the current continuity equation was very small. Since the high interface velocity on the ridge is an intrinsic effect of interface curvature, additional phenomena, which can provide suppression of ionic conduction near the ridge, must be

considered in order to fully explain the time-invariance of the PAA geometry. To this end, the concentration distribution of incorporated acid anions was simulated in conjunction with the current continuity model. Predictions followed experimentally observed distributions. Future work will develop mechanisms by which anions can inhibit conduction near the ridge, thus promoting uniform interface motion.

Acknowledgments

Financial support was provided by St. Jude Medical Corporation.

References

1. F. Keller, M. S. Hunter and D. L. Robinson, *J. Electrochem. Soc.,* **100,** 411 (1953).
2. J. W. Diggle, T. C. Downie and C. W. Goulding, *Chem. Rev.,* **69,** 365 (1969).
3. G. E. Thompson and G. C. Wood, in *Treatise on Materials Science and Technology,* Vol. 23, p. 205, J. C. Scully, Editor, Academic, New York (1983).
4. J. P. O'Sullivan and G. C. Wood, *Proc. Roy. Soc. London A.,* **317,** 511 (1970).
5. T. P. Hoar and N. F. Mott, *J. Phys. Chem. Solids,* **9,** 97 (1959).
6. A. P. Li, F. Müller, A. Birner, K. Nielsch, and U. Gösele, *J. Appl. Phys.,* **84,** 6023 (1998).
7. V. P. Parkhutik and V. I. Shershulsky, *J. Phys. D.: Appl. Phys.,* **25,** 1258 (1992).
8. S. K. Thamida and H.-C. Chang, *Chaos,* **12,** 240 (2002).
9. G. K. Singh, A. A. Golovin, I. S. Aranson, and V. M. Vinokur, *Europhys. Lett.,* **70,** 836 (2005).
10. K. Ebihara, H. Takahashi, and M. Nagayama, *J. Met. Finish. Soc. Japan,* **35,** 205 (1984).
11. J. E. Houser and K. R. Hebert, *J. Electrochem. Soc.,* **153,** B566 (2006).
12. S. Ono, M. Saito, M. Ishiguro, and H. Asoh, *J. Electrochem. Soc.*, **151**, B473 (2004).
13. G. E. Thompson and G. C. Wood, *Nature,* **290,** 230 (1981).
14. V. P. Parkhutik, *Corros. Sci.,* **26,** 295 (1986).
15. S. Ono and N. Masuko, *Corros. Sci.,* **33,** 503 (1992).
16. J. P. S. Pringle, *J. Electrochem. Soc.,* **120,** 398 (1973).
17. J. P. S. Pringle, *J. Electrochem. Soc.,* **120,** 1391 (1973).
18. K. Shimizu, G. M. Brown, H. Habazaki, K. Kobayashi, P. Skeldon, G. E. Thompson, and G. C. Wood, *Corros. Sci.,* **41,** 1971 (1999).
19. K. Shimizu, H. Habazaki, P. Skeldon, G. E. Thompson, and G. C. Wood, *Electrochim. Acta,* **45,** 1805 (2000).
20. K. Shimizu, H. Habazaki, P. Skeldon, G. E. Thompson, and G. C. Wood, *Electrochim. Acta,* **46,** 4379 (2001).
21. B. C. Bunker, G. C. Nelson, K. R. Zavadil, J. C. Barbour, F. D.Wall, J. P. Sullivan, C. F. Windlisch, Jr., M. H. Engelhardt and D. R. Baer, *J. Phys. Chem. B.,* **106,** 4705 (2002).
22. D. R. Jennison, P. A. Schultz and J. P. Sullivan, *Phys. Rev. B.,* **69,** 041405 (2004).
23. J. Choi, Y. Luo, R. B. Wehrspoon, R. Hillebrand, J. Schilling, and U. Gösele, *J. Appl. Phys.,* **94,** 4757 (2003).